Available online www.jocpr.com

Journal of Chemical and Pharmaceutical Research, 2012, 4(12):5126-5138

Research Article

ISSN : 0975-7384
CODEN(USA) : JCPRC5

Molecular structure and spectral analysis of 4-(2-pyridyl) benzaldehyde: A combined experiment and DFT approach

S. Ramachandran and G. Velraj*

Department of Physics, Periyar University, Salem 636 011, Tamil Nadu, India

---

ABSTRACT

In the present studies, the vibrational spectral analysis was carried out by FT-IR and FT-Raman spectroscopy in the range 3500-400 cm^{-1} and 3500-100 cm^{-1} for 4-(2-Pyridyl) benzaldehyde (42PBD) molecule, respectively. The molecular structure, fundamental vibrational frequencies and intensity of the vibrational bands are interpreted with the help of structure optimizations by density functional theory (DFT) method and B3LYP/ 6-311++G(d,p) basis set. The results of the calculations were applied to simulated spectra of the title compound, which showed good agreement with observed spectra. The ultraviolet visible (UV–VIS) absorption spectra of the studied compound dissolved in water, ethanol and methanol were examined in the wavelength range of 190–400 nm. The energy and oscillator strength calculated by time-dependent density functional theory (TD-DFT) complements with the experimental findings. In addition, frontier molecular orbitals (FMO), molecular electrostatic potential (MEP) and Mulliken atomic charge were determined. Thermodynamic properties of the title compound at different temperatures have been calculated.

Keywords: FT-IR; FT-Raman; DFT; TD-DFT; 4-(2-Pyridyl) Benzaldehyde.

INTRODUCTION

The Benzaldehyde is a raw material in medicine, dyestuff, spices and resin industry, mainly be used in the manufacture of lauryl aldehyde, lauric acid, plasticizer and low temperature lubricant. The majority of benzaldehyde reactions are taken place in solvent environment, solvent effects can be divided into specific effects and non-specific effects which play an important role in the chemical equilibrium, the rate of the chemical reaction and the reaction activity of benzaldehyde. As connecting directly to benzene ring and forming a large conjugate system, the carbonyl group of benzaldehyde is sensitive to the change of the surroundings [1,2]. Substituted benzaldehydes such as vanillin, p-hydroxybenzaldehyde, p-chlorobenzaldehyde, anisaldehyde are used in the synthesis of biologically active polymers, for example, in Chitosan derivatives, which are known for application in cosmetics, textiles, as biomaterials and for anti-microbial activity [3]. Benzaldehyde and acetophenone derivatives treated with base to form a substituted chalcone, which has been found to have anti-cancer properties [4]. Several workers have investigated vibrational spectroscopic properties, mutual influence of different types of substituents such as halogens, methyl, methoxy, Fluoro and hydroxyl through the benzaldehyde, the interactions between the ring and substituents, by the joint experimental and/or theoretical methods [5-13]. The best of our knowledge, complete vibrational assignments based on FT-IR and FT-Raman using DFT calculations are not available in the literature for the title compound under investigation. As a result we set out experimental and theoretical investigation of the vibrational and UV spectra of this molecule. Quantum chemical computational methods have proved to be an essential tool for interpreting and predicting the vibrational spectra [14,15].

The aim of the present work is to describe and characterize the molecular structure, vibrational and electronic properties of the title compound. A comparison of the experimental and theoretical spectra can be very useful in making correct assignments and understanding the molecular structure relationship. Molecular electrostatic potential

(MEP), frontier molecular orbitals (FMO), Mulliken atomic charge and thermodynamic parameters of the title compound were studied at the B3LYP/ 6-311++G(d,p) level.

EXPERIMENTAL SECTION

2. Experimental details

The compound under investigation namely 42PBD is purchased from Sigma–Aldrich chemicals and used for recording the spectra as such without any further purification. The FT-IR spectrum of the compound was recorded in Bruker Tensor 27 spectrometer in the range of 3500–400 cm^{-1}. The spectral resolution is 2 cm^{-1}. FT-Raman spectrum of the sample was recorded using 1064 nm line of Nd:YAG laser as excitation wavelength in the spectral region 3500–100cm^{-1} on Bruker RFS-27 FT-Raman spectrometer. The detector is a liquid nitrogen cooled germanium detector. The spectral resolution of 4 cm^{-1} using a laser power of 100 mW. The ultraviolet visible (UV-VIS) absorption spectra of the compound, which dissolved in water, ethanol and methanol, were examined in the range of 190–400 nm using Perkin Elmer Lambda 25 UV–VIS Spectrophotometer.

3. Computational details

The density functional theory (DFT) calculations with a hybrid functional B3LYP (Becke's three parameter hybrid functional using the LYP correlation functional) at 6-311++G(d,p) basis set were performed with the Gaussian 03W software package [16] and Gauss view visualization program [17]. UV–VIS spectra, electronic transitions, absorbance, oscillator strengths and electronic properties such as HOMO and LUMO energies were determined by time-dependent DFT (TD-DFT) approach.

The Molecular electrostatic potential (MEP) evaluated using the B3LYP/6-311++G(d,p) method. MEP, $V(r)$, at a given point $r(x, y, z)$ in the vicinity of a molecule, is defined in terms of the interaction energy between the electrical charge generated from the molecule's electrons, nuclei and a positive test charge (a proton) located at r. The values of $V(r)$ were calculated as described previously using the following equation [18]:

$$V(r) = \sum \frac{Z_A}{|R_A - r|} - \int \frac{\rho(r')}{|r' - r| d^3 r'} \qquad (1)$$

where Z_A is the charge of nucleus A, located at R_A, $\rho(r')$ is the electronic density function of the molecule and r' is the dummy integration variable.

3.1 Prediction of Raman intensities

The Raman activities calculated with Gaussian 03 program converted to relative Raman intensities using the following relationship derived from the intensity theory of Raman scattering [19,20]:

$$Ii = \frac{f(\upsilon_0 - \upsilon_i)^4 S_i}{\upsilon_i [1 - \exp(-hc\upsilon_i / kT)]} \qquad (2)$$

where υ_0 is the laser exciting wavenumber in cm^{-1} (in this work, we have used the excitation wavenumber υ_0 = 9398.5 cm^{-1}, which corresponds to the wavelength of 1064 nm of a Nd:YAG laser), υ_i the vibrational wavenumber of the ith normal mode (cm^{-1}), while *Si* is the Raman scattering activity of the normal mode υ_i. f (is a constant equal to 10^{-12}) is a suitably chosen common normalization factor for all peak intensities. *h*, *k*, *c* and *T* are Planck and Boltzmann constants, speed of light and temperature in Kelvin, respectively. Next, the spectra were analysed in terms of the potential energy distribution (PED) contributions by using the vibrational energy distribution analysis (VEDA) program [21].

RESULTS AND DISCUSSION

4.1. Structural analysis

The optimized structural parameters bond length and bond angle of the title compound were obtained using the B3LYP/6-311++G(d,p) level. The optimized parameters are presented in Table 1 in accordance with the atom numbering scheme of the molecule shown in Figure 1. The global energy minimum obtained by DFT of the structure optimization was -592.8240002a.u. and showed that the molecule belongs to *Cs* symmetry point group.

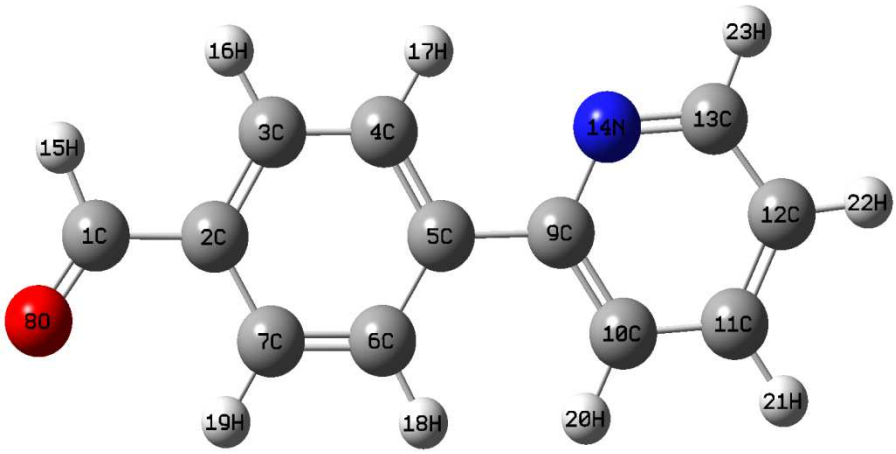

Figure 1. Optimization structure and atoms numbering of 42PBD.

Table 1. Optimized geometric data for 42PBD using B3LYP/3LYP/6–311++G(d,p).

Bond length	Value (Å)	Bond angle	Value (°)	Bond angle	Value (°)
C_1–C_2	1.4783	C_2–C_1–O_8	125.0508	C_9–C_{10}–C_{11}	119.4309
C_1–O_8	1.2118	C_2–C_1–H_{15}	114.4762	C_9–C_{10}–H_{20}	121.1487
C_1–H_{15}	1.1115	O_8–C_1–H_{15}	120.473	C_{11}–C_{10}–H_{20}	119.4204
C_2–C_3	1.3994	C_1–C_2–C_3	119.8758	C_{10}–C_{11}–C_{12}	119.1231
C_2–C_7	1.4005	C_1–C_2–C_7	121.0195	C_{10}–C_{11}–H_{21}	120.0766
C_3–C_4	1.3881	C_3–C_2–C_7	119.1047	C_{12}–C_{11}–H_{21}	120.8003
C_3–H_{16}	1.0859	C_2–C_3–C_4	120.6638	C_{11}–C_{12}–C_{13}	117.7003
C_4–C_5	1.404	C_2–C_3–H_{16}	119.5349	C_{11}–C_{12}–H_{22}	121.7176
C_4–H_{17}	1.0814	C_4–C_3–C_{16}	119.8013	C_{13}–C_{12}–H_{22}	120.5822
C_5–C_6	1.4075	C_3–C_4–C_5	120.6418	C_{12}–C_{13}–N_{14}	123.6586
C_5–C_9	1.4903	C_3–C_4–H_{17}	120.8913	C_{12}–C_{13}–H_{23}	120.3769
C_6–C_7	1.3858	C_5–C_4–H_{17}	118.4669	C_{14}–C_{13}–H_{23}	115.9645
C_6–H_{18}	1.0824	C_4–C_5–C_6	118.2888	C_9–N_{14}–C_{13}	119.0398
C_7–H_{19}	1.0837	C_4–C_5–C_9	119.4731		
C_9–C_{10}	1.4036	C_6–C_5–C_9	122.2381		
C_9–N_{14}	1.345	C_5–C_6–C_7	121.0775		
C_{10}–C_{11}	1.3897	C_5–C_6–H_{18}	120.5444		
C_{10}–H_{20}	1.0814	C_7–C_6–H_{18}	118.3781		
C_{11}–C_{12}	1.391	C_2–C_7–C_6	120.2234		
C_{11}–H_{21}	1.0843	C_2–C_7–H_{19}	118.8192		
C_{12}–C_{13}	1.3937	C_6–C_7–H_{19}	120.9573		
C_{12}–H_{22}	1.0831	C_5–C_9–C_{10}	122.5959		
C_{13}–N_{14}	1.331	C_5–C_9–N_{14}	116.3568		
C_{13}–H_{23}	1.0869	C_{10}–C_9–N_{14}	121.0473		

4.2. Vibrational spectra

From the structural point of view, the title molecule is assumed to have *Cs* point group symmetry. The molecule consists of 23 atoms, hence undergoes $\Gamma 3N\text{-}6_{vib}$=43*A′* + 20*A″* normal modes of vibrations. The vibrations of the *A′* species are in the plane and those of the *A″* species are out-of-plane. For visual comparison, observed FT-IR and FT-Raman spectra of 42PBD are shown in Figures 2 and 3, respectively. As a whole, the calculated spectra are more regular than the observed FT-IR and some bands found in the predicated IR spectra were not observed in the experimental spectra, as shown in Table 2. This is due to the fact that many vibrations presenting in condensed phase lead to strong perturbation of infrared intensities of many other modes. The aromatic C-H stretching vibrations were normally found between 3100 and 3000 cm^{-1} [22,23]. The aromatic C–H stretching vibrations of the title compound are observed at 3349 and 3076 cm^{-1} in the FT-IR and FT-Raman spectra. The antisymmetric stretching vibrations are observed at 3055 and 3059 cm^{-1} in the FT-IR and FT-Raman spectra, respectively. The calculated C–H stretching vibrations values are 3214, 3159 and 3145cm^{-1}. The bands due to C–H in-plane bending vibrations are observed in the region 1000–1300cm^{-1} [24]. For this compound, the C–H in-plane bending vibrations were observed at in the region 1100-1465cm^{-1} in FT-IR observed values at 1464, 1429, 1383, 1208, 1159, 1154, 1101cm^{-1} and 1411, 1292, 1211, 1172, 1154, 1062 cm^{-1} in FT-Raman. This mode was calculated in the range 1499–1053 cm^{-1}.

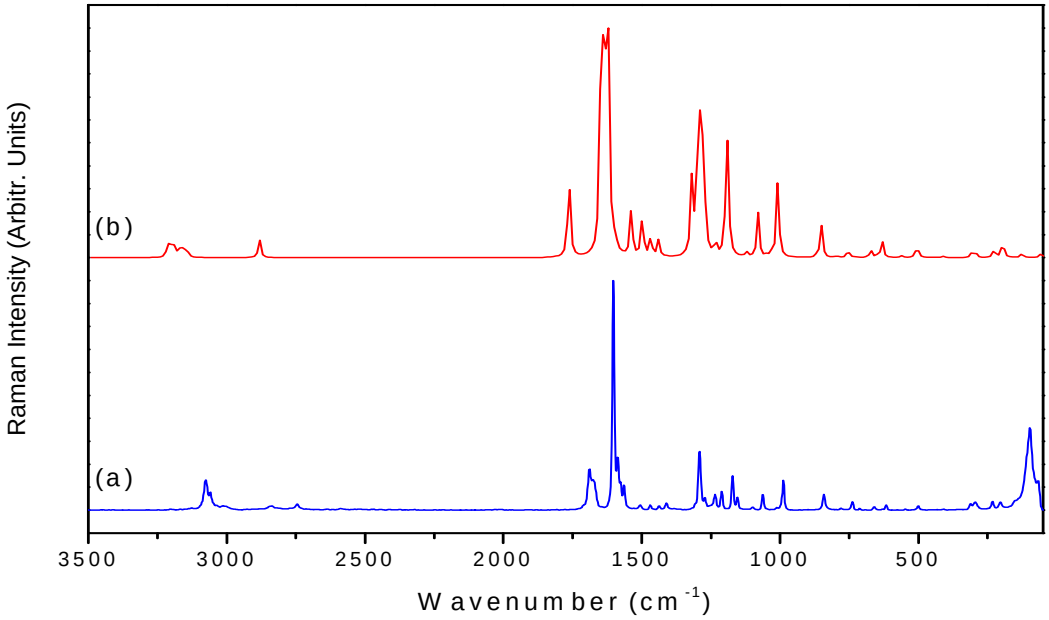

Figure 2. FT-IR spectrum: (a) observed; (b) 6-311++G(d,p).

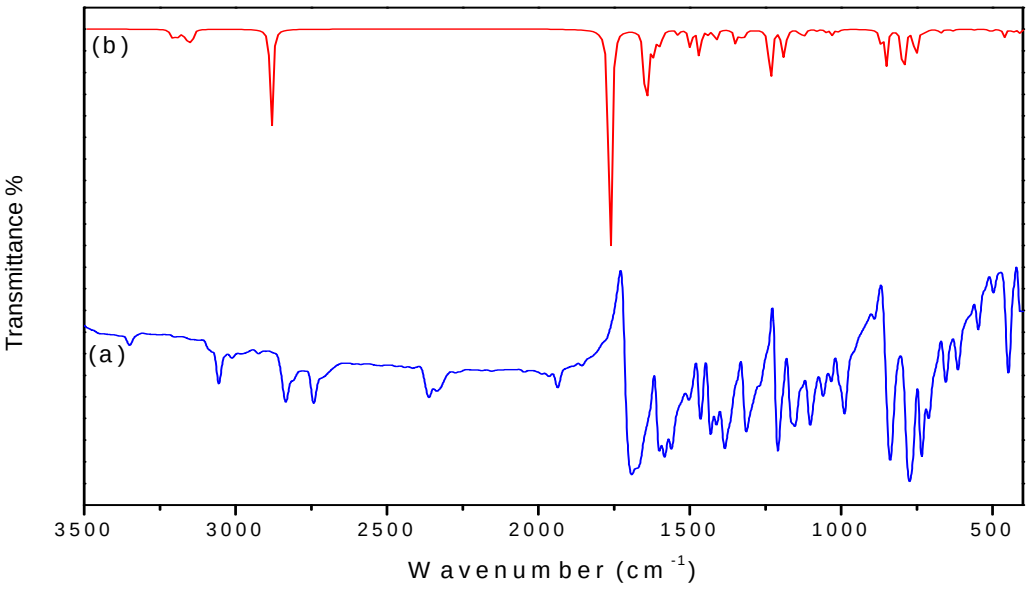

Figure 3. FT-Raman spectrum: (a) observed; (b) 6-311++G(d,p).

Table 2. Detailed assignments of fundamental vibrations of 42PBD.

Modes no	Experimental frequency(cm^{-1})[a]		Calculated frequency(cm^{-1}) B3LYP/6–311++G(d,p)				Vibrational Assignments(PED)[b]
	FT–IR	FT–Raman	Scaled value	IR Intensity	Raman Active	Raman Intensity	
	3349vs	–					Overtone + combination
A′	–	–	3134	0.99	80.76	0.013	υ C–H (96)
A′	–	–	3130	9.65	128.56	0.024	υ C–H (98)
A′	–	–	3118	1.75	34.57	0.003	υ_s C–H (92)
A′	–	–	3115	14.98	252.91	0.042	υ_{as} C–H (92)
A′	–	–	3103	1.97	22.52	0.004	υ_{as} C–H (90)
A′	–	–	3093	8.41	120.37	0.025	υ_{as} C–H (86)
A′	–	3076vw	3081	10.73	94.03	0.016	υ C–H (92)
A′	3055m	3059vw	3067	25.93	137.98	0.027	υ_{as} C–H (86)
A′	2833w	–	2808	137.82	193.70	0.048	υ C–H (90)
	–	1989w					Overtone + combination
A′	1698vw	–	1718	402.93	315.54	0.259	υ C=O (66)+ β C–H (18)
A′	1691vw	–	1603	152.66	1004.13	0.906	υ_s C–C (74)
A′	1596vw	1587vs	1584	27.35	1080.10	1.02	υ_s C–C (68) + υ C–N (21)
A′	–	–	1575	25.38	46.30	0.044	υ_s C–C (58) + υ C–N (24)
A′	–	1564s	1556	26.90	39.11	0.036	υ_{as} C–C (78)
A′	–	–	1499	7.25	134.67	0.137	β C–H (72)
A′	1464w	–	1460	27.14	103.14	0.112	β C–H (46)
A′	1429w	–	1430	42.47	48.76	0.055	β C–H (51)
A′	–	1411vw	1404	5.68	38.09	0.046	β C–H (58)+υ_s C–C (20)
A′	1383w	–	1378	20.52	3.18	0.004	β C–H (44)
A′	1311w	–	1316	17.46	0.37	0.003	υ_{as} C–C (48)+β C–H (23)
A′	–	–	1300	13.84	4.39	0.007	β C–H (66)
A′	–	1292vw	1285	9.15	177.18	0.235	υ C–C (43)+υ C–N (21)
A′	–	–	1261	1.21	401.59	0.552	β C–H (72)
A′	–	1235vw	1245	0.58	251.80	0.353	υ C–N (49)+υ C–C (27)
A′	1208m	1211vw	1203	98.53	27.43	0.041	υ C–C (55)+β C–H (16)
A′	1159m	1172w	1162	40.24	229.72	0.362	β C–H (47)
A′	1154m	1154w	1151	7.72	18.51	0.026	β C–H (46)
A′	1101m	–	1106	9.46	1.58	0.007	β C–H (44)
A′	–	–	1092	7.09	5.84	0.014	β C–H (45)
A′	–	1062vw	1053	2.29	64.78	0.114	β C–H (51)
A′	–	–	1020	4.23	3.02	0.003	τ Ring (85)
A″	–	–	1004	1.33	3.99	0.008	γ C–H (61)
A′	–	–	1003	6.69	1.07	0.004	τ Ring (87)
A′	991m	988w	982	2.70	109.61	0.221	τRing (91)
A″	–	–	981	0.11	0.61	0.003	γ C–H (61)
A″	–	–	979	0.41	0.05	0.004	γ C–H (64)
A″	–	–	960	0.00	0.19	0.006	γ C–H (71)
A″	–	–	956	0.24	0.04	0.002	γ C–H (68)
A″	–	–	878	0.00	0.00	0.008	γ C–H (65)
A″	837vw	842vw	847	16.69	1.73	0.003	γ C–H (66)
A″	–	–	832	1.47	0.30	0.005	γ C–H (72)
A′	–	–	829	47.89	34.07	0.080	τ Ring (82)

A″	773vw	–	775	83.54	1.55	0.005	*β* C–H (64)
A′	734vw	739w	736	39.80	7.47	0.026	*τ* Ring (91)
A″	–	–	730	8.54	0.06	0.003	*γ* C–H (71)
A″	–	–	707	5.44	0.70	0.007	*γ* C–H (56)
A′	655m	–	656	5.52	6.07	0.025	*τ* Ring (86)
A′	–	–	630	0.33	1.91	0.002	*τ* Ring (81)
A′	615s	–	615	2.35	11.52	0.044	*τ* Ring (91)
A″	–	–	546	0.75	0.96	0.006	*γ* C–H (48)
A′	–	–	492	3.42	7.22	0.038	*β* C=O (38)+β C–H (17)
A″	448s	–	449	10.82	10.82	0.069	*τ* Ring (83)
A′	–	–	423	4.51	4.51	0.027	*β* C–H (37)+β C–C (21)
A″	–	–	407	0.07	0.07	0.008	*ω* Ring(91)
A″	–	–	399	5.25	0.47	0.006	*ω* Ring (87)
A″	–	295vw	298	2.58	1.81	0.015	*τ* Ring (83)
A′	–	–	285	2.25	1.36	0.014	*τ* Ring (84)
A′	–	232vw	220	4.64	1.85	0.025	*β* C=O (43) + β C–H (17)
A″	–	–	190	2.17	3.15	0.041	*γ* C–H (51)
A′	–	–	123	4.06	0.05	0.003	*β* C=O (47) + β C–H (18)
A″	–	96m	122	8.92	0.48	0.015	*γ* C=O (61)
A″	–	–	55	0.21	0.22	0.012	*γ* C–H (67)
A″	–	–	30	2.23	0.07	0.006	*γ* C–H (58)

[a]vs–very strong; s–strong; m–medium strong; w–weak; vw–very weak.

[b]τ– torsion; γ– out of plane bending; β– in plane bending; υ– stretching; υ_s–symmetric stretching; υ_{as}– antisymmetric stretching; ω– wagging; t–twisting.

The C–H out-of-plane bending vibrations are appeared within the region 900–675cm^{-1} [25]. The vibrations identified at 991, 837 and 734 cm^{-1} in FT-IR and 988, 842, 965, 739 cm^{-1} in FT-Raman are assigned to C–H out-of-plane bending for 42PBD. The ring carbon–carbon stretching vibrations occur in the region 1625–1430 cm^{-1} [26]. The stretching vibrational bands for C–C bond are observed at 1691, 1596, 1464 and 1429 cm^{-1} in the FT-IR spectrum and 1587, 1564 and 1411cm^{-1} in the FT-Raman spectrum. The calculated Vibrational values are 1645, 1596, 1467and 1414cm^{-1}, respectively. The C=O stretching vibration of the aldehyde groups give rise to bands at 1725 cm^{-1} [27]. The C=O stretching vibration of 42PBD is observed at 1698cm^{-1} in FT-IR. The C=O in plane bending vibration is at 232 cm^{-1} in FT-Raman Spectrum.

4.3 UV–VIS spectrum

The electronic absorption spectra of title molecule were measured in water, ethanol and methanol at room temperature (298K). The excitation energies, absorbance and oscillator strengths for the title molecule at the optimized geometry in the ground state were obtained in the framework of TD-DFT calculations with the B3LYP/6-311++G(d,p) method. It is obvious that to use TD-DFT calculations to predict the electronic absorption spectra is a quite reasonable method. The calculated electronic transitions of high oscillatory strength are given in Table 3.

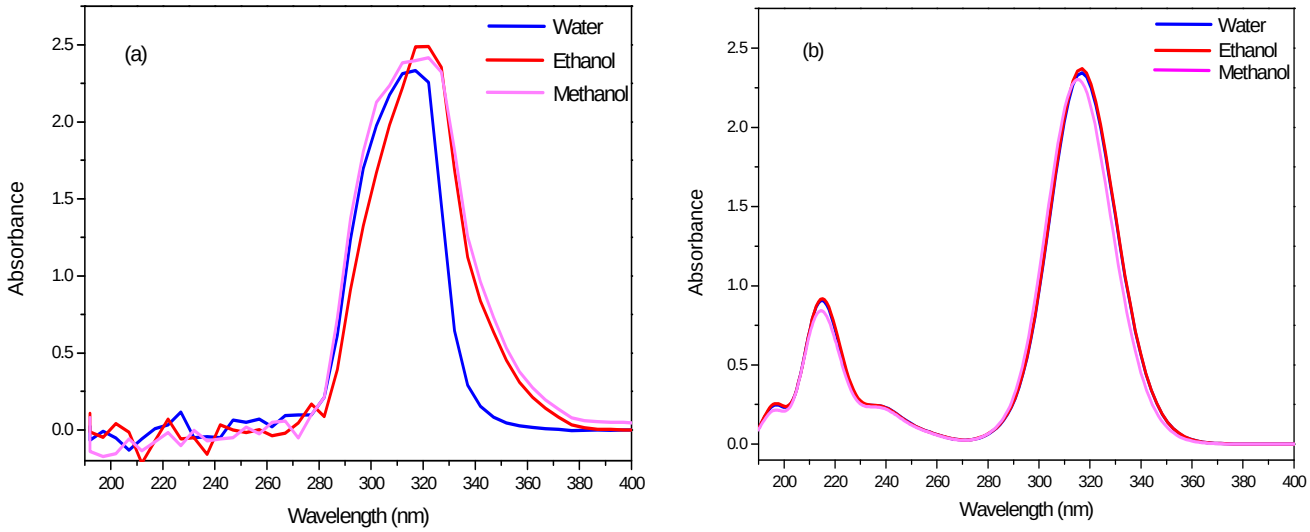

Figure 4. UV-Vis spectrum: (a) (a) observed; (b) 6-311++G(d,p).

Table 3. Experimental and calculated absorption wavelength λ (nm), excitation energies *E* (eV) and oscillator strengths (*f*) 42PBD of calculated by the B3LYP method using 6–311++G(d,p) basis set.

Medium	Experimental			TD–DFT (B3LYP)/6–311++G(d,p)			
	λ (nm)	*E* (eV)	Abs.	Major Contribution[a]	λ (nm)	*E* (eV)	*f*(a.u)
Water	317	3.912	2.33	H→L (85%)	316	3.925	0.8052
Ethanol	322	3.851	2.49	H→L (86%)	316	3.925	0.8141
Methanol	321	3.863	2.41	H→L (85%)	315	3.937	0.7904

[a]*for solvent phase (≥30); H, HOMO; L, LUMO.*

TD-DFT methods are computationally more expensive than semi-empirical methods but allow easily studies of medium size molecules [28,29]. Briquet and Vercauteren reported that TD-DFT λ_{max} calculations by 6-311++G(d,p) basis set is compatible with experimental results [30]. Test calculations have shown that the inclusion of extra polarization functions does not affect the excitation energies, besides the addition of diffuse functions leads to an increase in computation time. Experimentally determined maximum absorption values are 317 nm (in water), 322 nm (in ethanol) and 321 nm (in methanol). The λ_{max} values obtained with B3LYP/6-311++G(d,p) are 316 nm (in water), 316 nm (in ethanol) and 315 nm (in methanol). The experimental and calculated absorption spectra are shown in Figure. 4. The calculated and experimental λ_{max} values are agreed with each other.

4.4 Frontier molecular orbital analysis

The frontier molecular orbitals play an important role in the electronic and optical properties, as well as in UV-VIS spectra and chemical reactions [31]. The TD-DFT calculated electronic absorption spectra, the maximum absorption wavelength corresponding to the electronic transition is from the highest occupied molecular orbital (HOMO) to the lowest unoccupied molecular orbital (LUMO). The frontier molecular orbital energies of the title compound are shown in Figure. 5.

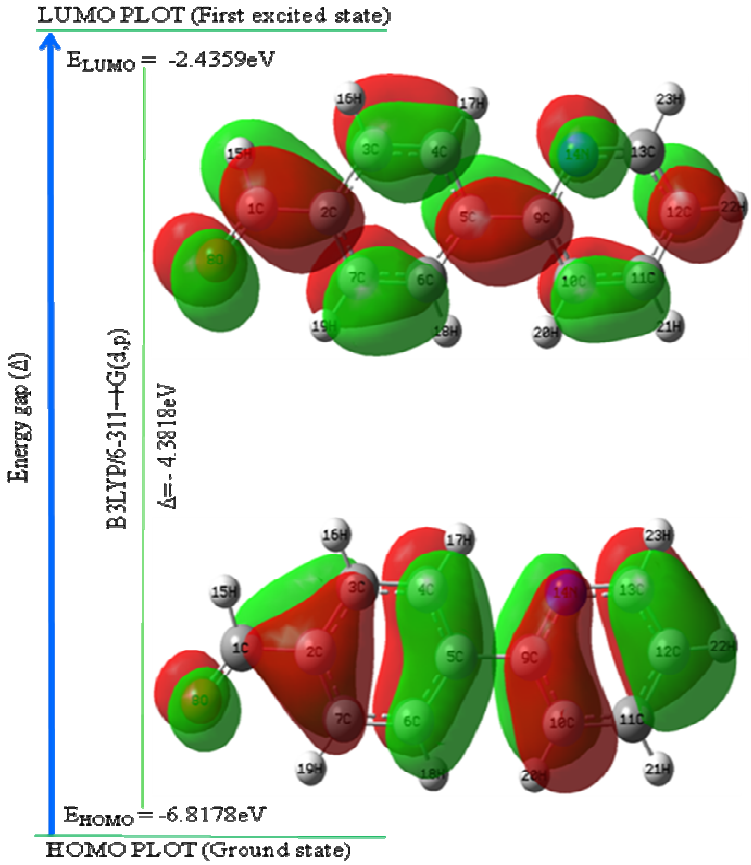

Figure 5. Atomic orbital composition of the frontier molecule for 42PBD.

The energy gap between HOMO and LUMO is a critical parameter in determining molecular electrical transport properties [32,33]. The lowest unoccupied molecular orbital (LUMO) energy is -2.4359 eV and the highest occupied molecular orbital (HOMO) energy is -6.8178 eV. The energy gap of HOMO–LUMO explains the ultimate charge transfer interaction within the molecule, and the frontier orbital energy gap of 42PBD is found to be -4.3818 eV obtained at TD−DFT method using 6-311++G(d,p) basis set. This large HOMO–LUMO gap automatically means high excitation energies for many of the excited states, good stability and a large chemical hardness for the title compound. The calculate ionization energy and electron affinity that can be expressed through HOMO and LUMO orbital energies as $I = -E_{HOMO}$ and $A = -E_{LUMO}$. The global hardness is $\eta = 1/2(E_{LUMO} - E_{HOMO})$. The hardness has been associated with the stability of chemical system. The electron affinity can be used in combination with ionization energy to give electronic chemical potential, $\mu = 1/2(E_{HOMO} + E_{LUMO})$. The global electrophilicity index, $\omega = \mu^2/2\eta$, is also calculated and listed in Table 4.

Table 4. Comparison of HOMO, LUMO, energy gaps (HOMO – LUMO) and related molecular properties of 42PBD (eV).

Molecular Energy	B3LYP/6–311++G(d,p)
E_{HOMO}	–6.8178
E_{LUMO}	–2.4359
Energy gap(Δ)	4.3818
Ionisation Potential (I)	6.8178
Electron affinity(A)	2.4359
Global Hardness (η)	2.1909
Chemical potential (μ)	–4.6268
Global Electrophilicity (ω)	4.8854

4.5 Molecular Electrostatic Potential

The 3D plots of molecular electrostatic potential (MEP) is a useful quantity to illustrate the charge distributions of molecules that are used to Visualize variably charged regions of a molecule. The MEP is a useful property to study reactivity given that an approaching electrophile will be attracted to negative regions (where the electron distribution effect is dominant). In the majority of the MEPs, while the maximum negative region which preferred site for electrophilic attack indications as red colour, the maximum positive region which preferred site for nucleophilic attack symptoms as blue colour. The MEP map (Figure. 6) shows that oxygen and nitrogen atoms represent the most negative potential region (dark red). The nitrogen atom seems to exert comparatively small negative potential as compared to oxygen atom. The predominance of green region in the MEP surface corresponds to a potential halfway between the two extremes red and dark blue colour [25].

The different values of the electrostatic potential at the surface are represented by different colours. Potential increases in the order red < orange < yellow < green < blue. The colour code of these maps is in the range between −5.270 kcal/mol (deepest red) and +5.270 kcal/mol (deepest blue) in compound, where blue indicates the strongest attraction and red indicates the strongest repulsion. Regions of negative $V(r)$ are usually associated with the lone pair of electronegative atoms. As can be seen from the MEP map of the title molecule, while regions having the negative potential are over the electronegative atom (O_8), the regions having the positive potential are over the hydrogen atoms.

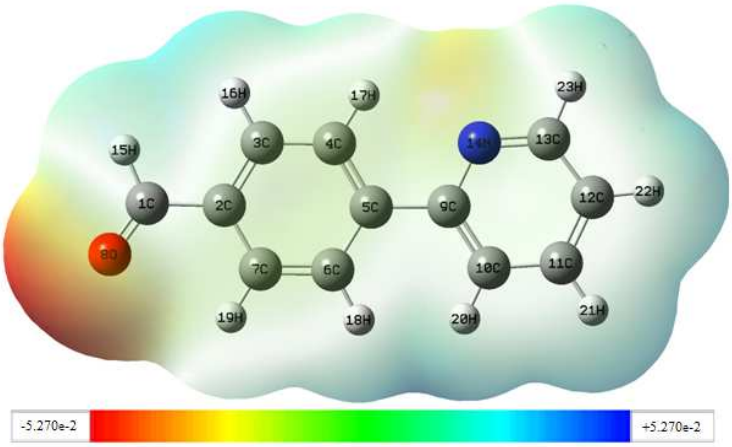

Figure 6. Molecular electrostatic potentials of 42PBD (B3LYP/6-311++G(d,p), 0.0004 a.u., energy values –5.270 to +5.270(kcal/mol); colour coding: red (very negative), orange (negative), yellow (slightly negative), green (neutral), turquoise (slightly positive), light blue (positive), dark blue (very positive).

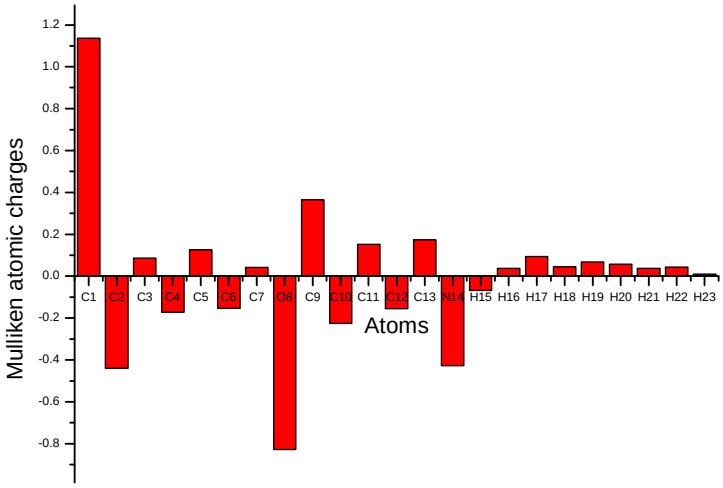

Figure. 7. The Mulliken charge of 42PBD molecule by using 6-311++G(d,p) basis set.

4.6 Mulliken atomic charge

The Mulliken atomic charge calculation has an important role in the application of quantum chemical calculation to molecular system because of atomic charges effect dipole moment, molecular polarizability, electronic structure and more a lot of properties of molecular systems. The atomic charges of 42PBD are calculated using B3LYP method with 6-311++G(d,p) basis set and the values are tabulated in Table 5. The more negative values on C_2, O_8, N_{14} atoms and more positive values are C_1, C_9, C_{13} atoms shown in Figure. 7.

Table 5. Mulliken atomic charges B3LYP/ 6–311++G(d,p)

Atoms	Mulliken atomic charges B3LYP/ 6–311++G(d,p)
C1	1.135674
C2	–0.4401
C3	0.086591
C4	–0.17229
C5	0.125987
C6	–0.15393
C7	0.042151
O8	–0.82771
C9	0.363964
C10	–0.22616
C11	0.152338
C12	–0.15623
C13	0.173494
N14	–0.4268
H15	–0.06821
H16	0.037513
H17	0.093738
H18	0.044033
H19	0.067443
H20	0.05762
H21	0.037439
H22	0.043157
H23	0.010273

4.7 Thermodynamic Properties

The values of some thermodynamic parameters such as zero point vibrational energy, thermal energy, specific heat capacity, rotational constants, entropy, and dipole moment of 42PBD by DFT/B3LYP with 6-311++G(d,p) method are listed in Table 6. On the basis of theoretical frequencies obtained from density functional calculations at B3LYP/6-311++G(d,p) level, the statistical standard thermodynamic functions: heat capacities ($C^0_{p,m}$), entropies (S^0_m) and enthalpy changes (ΔH^0_m) for the title compounds were obtained and are listed in Table 7. It is found that the standard heat capacities, entropies and enthalpy changes are increasing with temperatures ranging from 100 to 700 K due to the fact that the molecular vibrational intensities are increasing with temperatures [32,35].

Table 6. The calculated thermodynamic parameters of 42PBD employing B3LYP/ 6–311++G(d,p) methods.

Thermodynamic parameters (298K)	B3LYP/6–311++G(d,p)
SCF energy (a.u.)	–592.8240002
Total energy (thermal), E_{total} (kcal mol^{-1})	117.977
Heat capacity at const. volume, C_v (cal mol^{-1} K^{-1})	34.357
Entropy, S (cal mol^{-1} K^{-1})	26.047
Vibrational energy, E_{vib} (kcal mol^{-1})	116.200
Zero–point vibrational energy, E_0 (kcal mol^{-1})	111.70576
Rotational constants (GHz)	
A	2.75031
B	0.31497
C	0.28261
Dipole moment (Debye)	
μ_x	1.2735
μ_y	4.5609
μ_z	–0.3621
μ_{total}	4.7492

Table 7. Thermodynamic properties at different temperatures at the B3LYP/6–311++G(d,p) level of 42PBD.

T(K)	$C^0_{p,m}$ (cal mol^{-1}K^{-1})	S^0_m (cal mol^{-1}K^{-1})	H^0_m (Kcal mol^{-1})
100	8.695	5.772	112.071
200	20.582	15.299	113.513
298.15	34.357	26.047	116.200
300	34.623	26.261	116.264
400	48.359	38.138	120.425
500	60.067	50.230	125.866
600	69.536	62.050	132.364
700	77.144	73.362	139.711

The correlation equations between heat capacities, entropies, enthalpy changes and temperatures were fitted by quadratic formula, and the corresponding fitting factors (R^2) for these thermodynamic properties are 0.99856, 0.99931 and 0.99971, respectively. The corresponding fitting equations are as follows and the correlation graphics of those shows in Figures. 8–10 and the corresponding fitting equations are given as follows:

$$C^0_{p,m} = -8.18518 + 0.16156T - 5.48693 \times 10^{-5}T^2 \qquad (R^2 = 0.99856) \qquad (3)$$

$$S^0_m = -5.01104 + 0.10032T + 1.77633 \times 10^{-5}T^2 \qquad (R^2 = 0.99931) \qquad (4)$$

$$\Delta H^0_m = 111.84087 - 0.00451T + 6.46988 \times 10^{-5}T^2 \qquad (R^2 = 0.99971) \qquad (5)$$

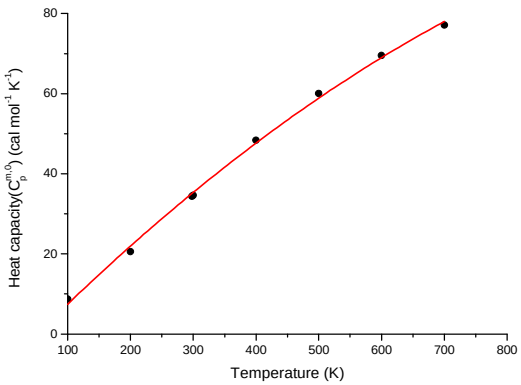

Figure 8. Correlation graph of heat capacity and temperature for 42PBD molecule.

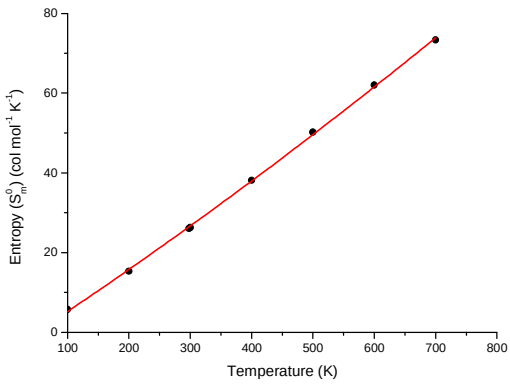

Figure 9. Correlation graph of entropy and temperature for 42PBD molecule.

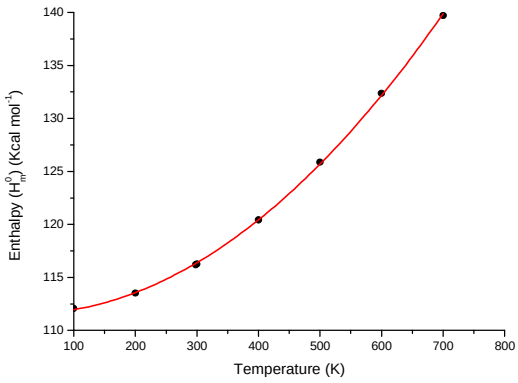

Figure 10. Correlation graph of enthalpy and temperature for 42PBD molecule.

They can be used to compute other thermodynamic energies from thermodynamic functions and can estimate the directions of chemical reactions according to the second law of thermodynamics in thermo chemical field [36]. All the thermodynamic data will be useful for further study on the 42PBD.

CONCLUSION

In the work, 4-(2-Pyridyl) Benzaldehyde (42PBD) was studied by spectroscopic (FT-IR and FT-Raman and UV-VIS) techniques. To support the solid state structure, the geometric parameters, vibrational frequencies, electric and thermodynamic property of the title compound have been calculated using the density functional theory (DFT/B3LYP) method with the 6−311G(d,p) basis set, and compared with the experimental findings. The value of the energy separation between the HOMO and LUMO is very large and this energy gap gives significant information about the title compound. The MEP map shows that the negative potential sites are on electronegative atoms and the positive potential sites are around the hydrogen atoms. These sites provide information concerning the region from where the compound can undergo intra and intermolecular interactions.

The correlations between the statistical thermodynamics and temperature are also obtained. It was seen that the heat capacities, entropies and enthalpies are increased with the increase in temperature due to the intensities of the molecular vibrations increase with increasing temperature.

Acknowledgment
One of the author, S. Ramachandran gratefully acknowledges Periyar University for providing financial assistance through University Research Fellowship (URF).

REFERENCES

[1] Q Liu; XY Wang; H Zhang, *Spectrochim. Acta A.*, **2007**, 66, 202–207.
[2] A Habibagahi; Y Mebarkib; Y Sultana; RJ Crutchley, *J. Photochem. Photobiol. A.*, **2011**, 225, 88– 94.
[3] ER Kenawy; F Imam Abdel-Hay; AA El-Magd; Y Mahmoud; *J. Bioactive Compatible Polym*., **2005**, 20, 95-111.
[4] CS Hirematha; J Tonannavar, *Spectrochim. Acta A.*, **2009**, 73, 388–397.
[5] D Singh; ID Singh; RA Yadav, *Ind. J. Phys.*, **2002**, 76B (1), 35-46.
[6] DN Singh; ID Singh; RA Yadav, *Ind. J. Phys.*, **2002**, 76B(3), 307-318.
[7] A Anjaneyulu; G Ramana Rao, *Spectrochim. Acta A.*, **1999**, 55, 749-760.
[8] P Venkata Raman Rao; G Ramana Rao, *Spectrochim. Acta A.*, **2002**, 58, 3205-3221.
[9] N Akai; S Kudoh; M Takayanagi; M Nakata, *J. Photochem. Photobiol. A.*, **2002**, 150, 93-100.
[10] T Drakenberg; R Jost; JM Sommer, *J. Chem. Soc., Perkin Trans*., **1975**, 2, 1682-1684.
[11] P Bednarek; T Bally; J Gebicki, *J. Org. Chem*., **2002**, 67, 1319-1322.
[12] T Itoh; N Akai; K Ohno, *J. Mol. Struct*., **2006**, 786, 39-45.
[13] O Prasad; A Kumar; V Narayan; HN Mishra; RK Srivastava; L Sinha, *J. Chem. Pharm. Res*., **2011**, 3(5):668-677.
[14] BA Hess; J Schaad; P Carsky; R Zahradnik, *Chem Rev.*, **1986**, 86, 709-730.
[15] P Pulay; X Zhou; G Fogarasi, Recent Experimental and Computational Advances in Molecular Spectroscopy, NATO ASI Series, Vol. C 406 (Ed.: R. Fransto), Kluwer, Dordrecht **1993;** 99-111.
[16] Gaussian Inc., Gaussian 03 Program, Gaussian Inc., Wallingford, **2004**.

[17] R Dennington; T Keith, J Millam, Gauss View Version 4.1 2, Semichem, Inc.,Shawnee Mission, KS, **2007**.
[18] P. Politzer; J.S. Murray, *Theor. Chem. Acc*., **2002**, 108, 134–142.
[19] G Keresztury; S Holly; G Besenyei; J Varga; A Wang; JR Durig, *Spectrochim Acta A.*, **1993**, 49, 2007-2017.
[20] G Keresztury, in: JM Chalmers, PR Griffith (Eds.), Raman Spectroscopy: Theory,
Hand book of Vibrational Spectroscopy, vol. 1, John Wiley & Sons Ltd, New York, **2002**.
[22] MH Jamroz, Vibrational Energy Distribution Analysis, VEDA 4, Warsaw, **2004.**
[22] DN Sathyanarayana, Vibrational Spectroscopy, Theory and Applications, New Age International (p) Limited Publishers, New Delhi, **2004**.
[23] S Muthu; EI Paulraj, *J. Chem. Pharm. Res*., **2011**, 3(5), 323-339.
[24] MH Jamroz, JC Dobrowolski, R Brzozowski, *J. Mol. Struct*., **2006**, 787, 172–183.
[25] M Govindarajan; M Karabacak, *Spectrochim. Acta A.*, **2012**, 85, 251– 260.
[26] M Silverstein; GC Basseler; C Morill, Spectrometric Identification of Organic Compounds, Wiley, New York, **1981**.
[27] R Asha; K Raju; HT Varghese; M Carlos; Granaderio; IS Helena; C Nogueiradand; Y Panicker, *J. Brazil. Chem. Soc*., **2009**, 20, 549-559.
[28] D Guillaumont; S Nakamura, *Dyes Pigments.*, **2000**, 46, 85–92.
[29] J Fabian, *Dyes Pigments*., **2010**, 84, 36–53.
[30] L Briquet; DP Vercauteren; JM Andre; EA Perpete; D. Jacquemin, *Chem. Phys. Lett*., **2007**, 435, 257–262.
[31] I Fleming, Frontier Orbitals and Organic Chemical Reactions Wiley, London, **1976**.
[32] K Fukui, Science., **1982**, 218, 747–754.
[33] P Udhayakala; TV Rajendiran; S Seshadri; S Gunasekaran, *J. Chem. Pharm. Res*., **2011**, 3(3), *610-625.*
[34] R Zhang, B Dub, G Sun, Y Sun, *Spectrochim. Acta A.*, **2010**, 75, 1115–1124.
[35] P Singh; NP Singh; RA Yadav, *J. Chem. Pharm. Res*., **2010**, 2(6):199-224.
[36] D Shoba; M Karabacak; S Periandy; S Ramalingam, *Spectrochim. Acta A.*, **2011**, 81, 504–518.